BMC Microbiology

RESEARCH

Open Access

Helicobacter pylori infection impairs glucose homeostasis through gut microbiota dysbiosis

Han Chen[1,2†], Zi Wang[1,2†], Wei Su[1,2†], Shuo Li[1,2], Qiang Ye[1,2], Guoxin Zhang[1,2*] and Xiaoying Zhou[1,2*]

Abstract

Background Epidemiological data show that *Helicobacter pylori* (*H. pylori*) infection is not only the most important risk factor for gastric cancer, but is also associated with poor glycemic control in patients with diabetes. However, the direct causal and functional relationship between *H. pylori* infection and dysglycemia is unclear.

Method A retrospective cohort study was conducted to examine the association between *H. pylori* infection and glycemic levels in individuals with Type 2 diabetes. C57BL/6 diabetic mice were infected with *H. pylori*, and the resulting changes in colonic inflammation and intestinal Glucagon-like peptide-1 (GLP-1) secretion were thoroughly examined using immunohistochemistry, RNA sequencing, metagenomic sequencing, and targeted metabolomics. The microbial and metabolomics profiles were analyzed and compared in antibiotic-treated mice through fecal transfer experiments.

Results *H. pylori* infection aggravated insulin resistance in diabetic individuals and mice. We identified a unique *H. pylori*-induced epithelial inflammation and reduced intestinal GLP-1 secretion in the colon. *H. pylori* infection also interrupts the normal microbial composition in the colon, leading to a decrease in SCFA-producing bacteria and a reduction in acetic and propionate acids. Similar changes were observed in antibiotic-treated mice after receiving fecal transplants from *H. pylori*-infected diabetic mice. In vitro studies revealed that the intestinal flora of *H. pylori*-positive diabetic mice inhibited proglucagon transcription, cAMP levels, and GLP-1 secretion in colonic endocrine cells, with SCFA supplementation reversing this effect on GLP-1 production. These microbial, metabolic, and GLP-1 alterations were also seen in antibiotic-treated mice after receiving fecal transplants from *H. pylori*-infected diabetic mice. *H. pylori* eradication with antibiotics improved glucose metabolism and GLP-1 secretion to levels comparable to uninfected controls.

Conclusion Our studies offer evidence that *H. pylori* infection significantly contributes to the progression of glucose impairment and insulin resistance. Therefore, incorporating *H. pylori* status into preventive strategies for diabetes should be taken into account. (Chinese Clinical Trial Registry Center, ChiCTR2200063489, Registered 08 September 2022, https://www.chictr.org.cn/showproj.html?proj=178102).

Keywords *Helicobacter pylori*, Type 2 diabetes, GLP-1, Gut microbiota, Insulin resistance

†Han Chen, Zi Wang and Wei Su contributed equally to this work.

*Correspondence:
Guoxin Zhang
zhangguoxinzxy@163.com

Xiaoying Zhou
zhouxiaoying0926@njmu.edu.cn
[1]Department of Gastroenterology, The First Affiliated Hospital of Nanjing Medical University, 300# Guangzhou Road, Nanjing 210029, P. R. China
[2]The First Clinical Medical College, Nanjing Medical University, Nanjing, China

Introduction

Helicobacter pylori (*H. pylori*) is a prevalent infectious pathogen with a global infection rate exceeding 50% [1], posing a significant health risk to Chinese residents. *H. pylori* is a well-established etiological agent for a range of gastric disorders and has also been associated with the pathogenesis of several extra-gastrointestinal conditions, including obesity, diabetes, and non-alcoholic fatty liver disease [2]. However, the precise pathogenic mechanism remains unclear. Among these, Type 2 Diabetes (T2D) is a common metabolic disease associated with *H. pylori* infection, characterized by insulin resistance and/or inadequate insulin secretion [3]. Numerous clinical studies have demonstrated that *H. pylori* infection can worsen insulin resistance in T2D [4–10]. In T2D patients, the prevalence of *H. pylori* infection is significantly higher compared to healthy individuals, with a lower eradication rate [4, 5]. *H. pylori* infection can exacerbate insulin resistance in T2D, leading to fluctuations in fasting and postprandial glucose levels [6–8]. Moreover, successful eradication of *H. pylori* has shown significant improvements in fasting blood glucose and glycated hemoglobin (HbA1c) levels in T2D patients [9, 10]. These findings collectively support the association between *H. pylori* and T2D. However, the existing evidence are primarily based on the findings of clinical cross-sectional or retrospective cohort studies. The presence of a bidirectional causal relationship between the two conditions has not been definitively elucidated.

H. pylori infection can lead to gastric microbial dysbiosis and a decrease in gastric microbiota diversity [11, 12]. Additionally, it can impact the composition of intestinal flora and cause an imbalance in the intestinal microecology [13]. This could be attributed to the disruption of the normal gastric environment by *H. pylori*, creating a pathway between the oral cavity and intestines that influences the intestinal flora [14]. Some researchers have suggested that the disruption caused by *H. pylori* on intestinal flora may contribute to the development of metabolic diseases by affecting the host's energy metabolism and hormone levels [15]. This, combined with the higher occurrence of clinical symptoms in T2D patients with *H. pylori*-positive status, implies that intestinal flora may serve as a link between *H. pylori* infection and metabolic diseases. Furthermore, studies have shown that *H. pylori* infection can impact the production of short chain fatty acids (SCFAs) in the intestine [16]. When comparing *H. pylori*-positive and negative mice, significant differences were observed in the intestinal bacteria and fecal SCFAs content. Interestingly, supplementing SCFAs did not significantly increase the fecal SCFAs content in *H. pylori*-positive mice, suggesting that SCFAs production may be more influenced by specific SCFA-producing bacteria rather than direct exogenous intake [16]. Therefore, it is hypothesized that *H. pylori* may affect the production of intestinal SCFAs by altering the abundance of SCFA-producing bacteria.

H. pylori not only impacts the intestinal microbial community and specific metabolites, but also influences the regulation of human metabolic hormones [17]. Glucagon-like peptide-1 (GLP-1) is an incretin hormone produced by enteroendocrine L-cells, stimulating insulin secretion by pancreatic β-cells [18] and participating in food intake and energy metabolism to maintain glucose homeostasis [19, 20]. Research indicates that eradication of *H. pylori* can elevate GLP-1 secretion levels, as demonstrated in clinical studies [17, 21]. Cornejo-Pareja et al. observed increased GLP-1 secretion and improved carbohydrate metabolism post-eradication. Changes in intestinal microecology post-eradication may contribute to GLP-1 secretion regulation [21]. Similarly, Yap et al. reported a gradual rise in GLP-1 levels at 0, 6, and 12 months post-eradication [17]. However, further research is needed to determine if fluctuations in GLP-1 levels post-*H. pylori* infection or eradication impact insulin resistance in type 2 diabetes.

In this study, we identified *H. pylori*-specific modifications in gut homeostasis that exacerbate insulin resistance, and these alterations are reversible upon eradication of *H. pylori*. These findings establish a foundation for exploring the molecular mechanisms by which *H. pylori* contributes to the development of metabolic diseases.

Methods and materials

Human retrospective cohort establishment

To investigate the correlation between *H. pylori* infection and the clinical blood glucose control level in patients with T2D, a retrospective cohort study was conducted on patients diagnosed with T2D between January 2017 and October 2021. Patients were categorized into two groups based on the results of the 13 C urease breath test (13C-UBT): *H. pylori* positive group and *H. pylori* negative group. Inclusion criteria consist of patients aged 18–75 who have been diagnosed with T2D (fasting blood glucose > 7.0 mmol/L and/or Oral Glucose Tolerance Test (OGTT) 2 h > 11.1 mmol/L) for a minimum of 6 months and have undergone a 13C-UBT following their T2D diagnosis. Exclusion criteria include patients with Type 1 diabetes, individuals who are children, pregnant, or lactating, as well as patients with a history of malignant tumors. The patient's age, gender, Body Mass Index (BMI) index, course and treatment plan for T2D, history of underlying diseases, *H. pylori* eradication status, and blood sugar-related indicators before and after eradication (including Fasting Blood Glucose (FBG), HbA1c, total cholesterol (TC), and total triglycerides (TG) were retrospectively collected. All clinical data

were obtained with the informed consent of the patient. The study received approval from the Institutional Ethics Committee of the First Affiliated Hospital of Nanjing Medical University (Ethics Number: 2022-SR-406) and was subsequently registered in the Chinese Clinical Trial Registry center (www.chictr.org.cn; registration No. ChiCTR2200063489, Registration Date: September 8, 2022). The detailed design and analysis in the human human retrospective cohort study were shown in the supplementary materials.

Pylori cultivation and infection

H. pylori Sydney strain (Hp-SS1) was cultured in Columbia medium at 37℃ in a three-gas incubator with microaerobic conditions (5% O2, 10% CO2, 75% N2). After 48 h, the bacteria were washed with Brucella broth, and the concentration of *H. pylori* was determined using a spectrophotometer. The concentration was adjusted to above 1 × 10^8 CFU/ml using a concentration and dilution method. Strain identification criteria were shown in the supplementary materials. For the in vivo model establishment, Brucella broth containing 10^8 −10^9 CFU/ml of *H. pylori* SS1 strain was orally administered at 0.01 ml/g for 4 weeks (the control group received an equal amount of Brucella broth). The success of the model establishment was evaluated by performing mouse fecal antigen detection kit (HpSA, 20,183,400,060, Richen biotech, Taizhou, China) in vivo. Additionally, after euthanasia, gastric antrum tissue was homogenized and plated on selective media. A colonization amount greater than 10^4 CFU/mg was considered positive; successful model establishment was confirmed if either of the two methods yielded positive results.

Animal studies

The animal studies were conducted in accordance with relevant ethical regulations and approved by the Institutional Animal Care and Use Committee (IACUC-2207010) at Nanjing Medical University. Wild-type C57BL/6J mice (male, four weeks old, Specific Pathogen-Free grade) were obtained from Beijing Vital River Laboratory Animal Technology Co., Ltd. and allowed two weeks of acclimatization. The mice were housed in individually ventilated cages under specific pathogen-free conditions, with free access to ultrapure water, and maintained at a controlled environment (22–25 °C, 12-h light/dark cycle). All mice experiments used either a standard chow diet (TP23522, Trophic Animal Feed High-tech Co., Ltd, China) or a high-fat diet (HFD: 60% kcal from fat; D12492, Research Diets). Detailed animal experiments design was shown in the supplementary materials. Mice were anesthetized with 1.5% isoflurane and sacrificed by cervical dislocation after tissue collection.

GLP-1 and insulin measurement

The levels of active GLP-1 were measured using an EZGLPHS-35K assay kit from Millipore, while HbA1c levels were measured using an enzymatic method with a Hitachi 7180 Clinical Analyzer (Hitachi, Tokyo, Japan) and Serum insulin levels were determined using mouse ELISA kits from Crystal Chem Inc. (90,080), following the manufacturer's instructions.

Histopathology and immunohistochemistry

Liver, colon, and pancreas tissues were fixed with 4% paraformaldehyde, embedded in paraffin, and then cut into 3 μm sections for hematoxylin–eosin staining or immunohistochemistry. Immunohistochemistry was performed using primary antibodies against CD3 (Servicebio, GB11014, 1:300), GLP-1R (Servicebio, GB113881, 1:300), and F4/80 (Servicebio, GB113373, 1:200). Quantitative analysis was conducted on randomly selected stained tissue sections to measure the area and number of positive cells. The expression levels were quantified digitally using Image J software (version 1.52).

Western blot

Proteins were extracted from colon tissue and underwent denaturing sodium dodecyl sulfate–polyacrylamide gel electrophoresis. The proteins were transferred to polyvinylidene difluoride membranes (MilliporeSigma, Burlington, MA, USA). After blocking with 5% milk for 1 h, the membranes were incubated overnight at 4 °C with primary antibodies targeting IRS-1 (Proteintech Group, Rosemont, IL, USA; 19,811–1-AP) and β-actin (Immunoway, YM3028). Post three washes with phosphate-buffered saline with Tween-20, the membranes were exposed to secondary antibodies for 1 h. Goat anti-rabbit IgG-HRP (Immunoway, RS0002) and goat anti-mouse IgG-HRP (Immunoway, RS0001) served as the secondary antibodies. Image J software (version 1.52) was utilized to quantify band intensities, which were then normalized to β-actin levels.

RNA sequencing analysis

Paired-end sequencing was conducted on the NovaSeq 6000 platform by Illumina through Wuhan Metware Biotechnology Cp. Ltd. FastQC (version 0.11.8) was used to evaluate raw data quality in FASTQ format, while the Cutadapt software (version 1.15) was utilized to obtain high-quality clean data. Read counting and FPKM calculation for expression standardization were performed using HTSeq (version 0.9.1). Following this, differential gene expression analysis and functional enrichment analysis of the samples were conducted.

Fecal sample collection

Fresh fecal samples (2–3 pellets) were collected by directly collecting the samples when the mouse defecated. This was done by first holding the mouse in one hand, transferring the sample with a disposable sterile plastic surgical tweezer (Cangzhou Hengbo Co., Ltd., Hebei, China) into a 2-ml sterile cryogenic vial (Corning Incorporated, USA), quickly placing the tube into a sealed sterile plastic bag, and then storing it in a – 80 °C environment until further processing.

DNA extraction and 16 S rRNA gene sequencing

The detailed method [22] for DNA extraction was shown in the supplementary materials. Raw data from the 16 s rRNA sequence was processed by Personalbio Technology Co., Ltd. (Shanghai, China). Amplicon sequence variants (ASVs) were integrated into merged taxonomic abundance and taxonomy classification tables. Linear discriminant analysis effect size (LEfSe) was calculated with the online website (http://huttenhower.sph.harvard.edu/galaxy) to determine significant biomarkers for colonic microbita of *H. pylori*-infected mice [23].

Metagenomic analysis

The raw data analysis was performed by Personalbio Technology Co., Ltd. (Shanghai, China), utilizing tools such as Cutadapt, KneadData, and FastQC for quality control of raw data (implemented through Trimmomatic), and Kraken2 along with a self-built microbial database for species annotation. The metagenomic raw data have been submitted to the Sequence Read Archive (SRA) in NCBI (https://www.ncbi.nlm.nih.gov/, number PRJNA1139859). The generated metagenomic data of mice were further analyzed using the MicrobiomeAnalyst (https://www.microbiomeanalyst.ca/) [24]. The manhattan plot was generated using metagenomeSeq and ggplot2 packages. Molecular ecological network analyses (MENAs) were applied to construct random matrix theory (RMT) based on co-occurrence bacterial networks using Spearman's correlation coefficient and presented in Grephi Version 0.9.5.

Cell culture and measurement

STC-1 and NCI-H716 cell lines were obtained from ATCC. STC-1 cells were of murine origin, while NCI-H716 cells were of human cecum origin. These cell lines were cultured in different media, with STC-1 cells cultured in DMEM medium and NCI-H716 cells cultured in RPMI 1640 medium. Both cell lines were supplemented with 10% fetal bovine serum and 1% penicillin–streptomycin and maintained at 37℃ in a 5% CO2 environment. The detailed design was shown in the supplementary materials.

Results

H. pylori infection aggravates glucose intolerance in patients with T2D

To investigate the relationship between *H. pylori* infection and glucose intolerance, a retrospective cohort of 389 patients with T2D was established, including 241 patients with positive *H. pylori* infection according to the 13C-UBT test and 189 controls (Figure S1A). Baseline characteristics are outlined in Table S1. Patients with *H. pylori* infection showed a significant increase in FBG (8.8 versus 7.5 mmol/L, $P < 0.001$), HbA1c (7.9% versus 6.8%, $P < 0.001$), total cholesterol (4.86 versus 4.55 mmol/L, $P = 0.013$), and low-density lipoprotein levels (3.05 versus 2.78 mmol/L, $P = 0.005$) compared to controls (Figure S1B-E). After successful eradication of *H. pylori*, there was a notable improvement in glucose control, with reductions in FBG (median difference: −1.2 mmol/L, $P < 0.001$) and HbA1c levels (median difference: −0.4%, $P < 0.001$). These results indicate that *H. pylori* infection could induce a potential disruption of glucose homeostasis.

H. pylori aggravates glucose intolerance and decreased serum GLP-1 levels in diabetic mouse model

To further investigate the impact of *H. pylori* infection on glucose homeostasis, C57 mice were induced with a high-fat diet and streptozotocin (HFD + STZ) and subsequently infected with *H. pylori* (Fig. 1A). The diabetic mice were then intragastrically administrated with 10^8 CFU/ml of *H. pylori SS1* strain or an equal amount of control medium (Brucella broth) every 72 h for four weeks. The in vitro and in vivo validation of *H. pylori* infection was shown in supplementary material and Figure S2A-G. The body weights in *H. pylori* infected mice slightly decreased during gavage but increased after 6 weeks of infection (Fig. 1B). *H. pylori* infection significantly increased the FBG and HOMA-IR compared with controls (Fig. 1C and D). Following *H. pylori* infection, diabetic mice exhibited significant impairments in glucose tolerance and insulin sensitivity (Fig. 1E and F). We further observed that *H. pylori*-infected diabetic mice had a higher daily calorie intake compared to control (Fig. 1G). Building on previous research showing the impact of GLP-1 on glucose regulation and appetite control [19, 20], we then tested the effects of *H. pylori* on the serum GLP-1 level. The results showed a significant decrease in active GLP-1 concentration 14 weeks after the start of *H. pylori* infection (Fig. 1H). To further investigate the impact of *H. pylori* infection on the liver, we conducted histological analysis of liver tissue using H&E staining, Oil-red O staining, and F4/80 immunohistochemistry. We observed notable microvesicular steatosis along with mild inflammation in diabetic mice compared to controls. Interestingly, the severity of hepatic fat

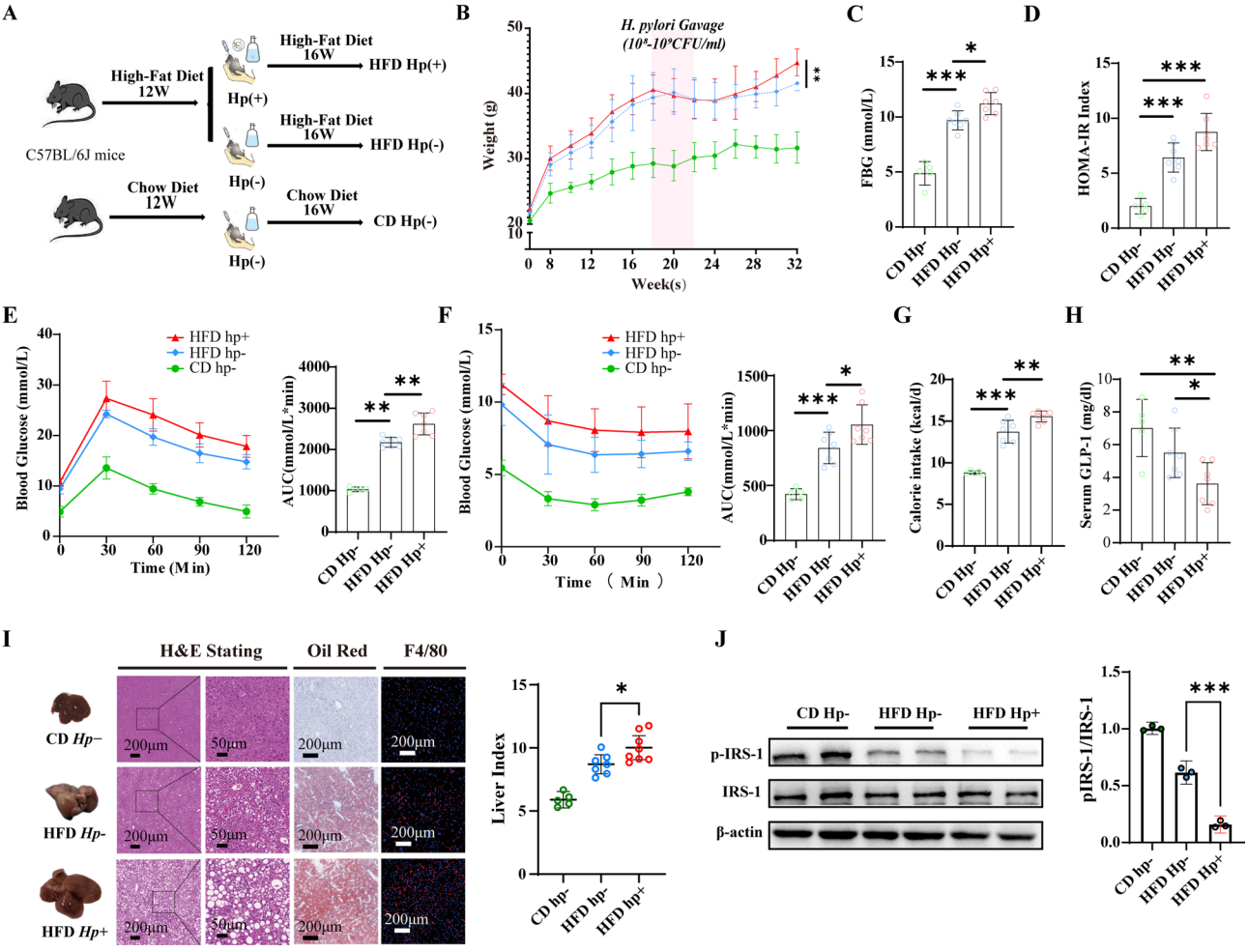

Fig. 1 *Helicobacter* pylori infection aggravates insulin resistance in HFD + STZ mouse model. **A** Schematic diagram of the animal study design; **B** body weight change during the animal experiment; **C** Fasting blood glusose level; **D** Homeostasis model assessment of insulin resistance (HOMA-IR) level, (FBG(mmol/L)*FINS(uU/mL)/22.5); **E** Blood glucose levels and AUC of OGTT; **F** blood glucose levels of ITT; **G** Daily calorie intake; **H** serum active GLP-1 levels; **I**. Representative images of gross appearance of the liver histology (1 cm) and photomicrographs of fixed liver sections after staining with H&E (50 μm and 200 μm), ORO (200 μm), F4/80 antibody (200 μm), and quantification of the liver index (%); J. IRS-1 and p-IRS-1 protein expression in the liver tissue. *$p < 0.05$, **$p < 0.01$, ***$p < 0.001$

accumulation worsened following *H. pylori* infection, and there was a significant increase in the number of infiltrating macrophages (F4/80-positive cells) and the liver index was also remarkably increased in the *H. pylori*-infected diabetic mice group (Fig. 1I). Given that insulin receptor substrate (IRS) 1 is involved in hepatic insulin signaling and is generally involved in the inhibition of gluconeogenesis and activation of lipogenesis, we then examined the expression levels of IRS1 and p-IRS1 in liver tissues and found that the ratio of IRS1/p-IRS1 was significantly increased in *H. pylori*-infected diabetic mice (Fig. 1J), suggesting that *H. pylori* infection further interrupt the hepatic insulin signaling and aggravates hepatic insulin resistance.

H. pylori exacerbates the intestinal epithelial inflammatory response and attenuates enterogenous GLP-1 secretions

Previous studies have indicated that *H. pylori* infection triggers a pro-inflammatory response in the intestine [25, 26]. Thus, we examined the effect of *H. pylori* infection on intestinal inflammation. Histological analysis of the intestines revealed that *H. pylori* infection led to significant damage in diabetic mice, as demonstrated by a shortened total colon length, increased histological colitis score, and dilated tight junctions observed under transmission electron microscopy (Fig. 2A, B, C). Since *H. pylori* infection influences the host T cell immune response contributing to gastric inflammation, we analyzed lymphocyte infiltration and observed an increased number of intraepithelial CD3 + T cells in both the stomach and colon upon *H. pylori* infection (Figure S2D, E). Furthermore, the examination of mucus-producing goblet cells

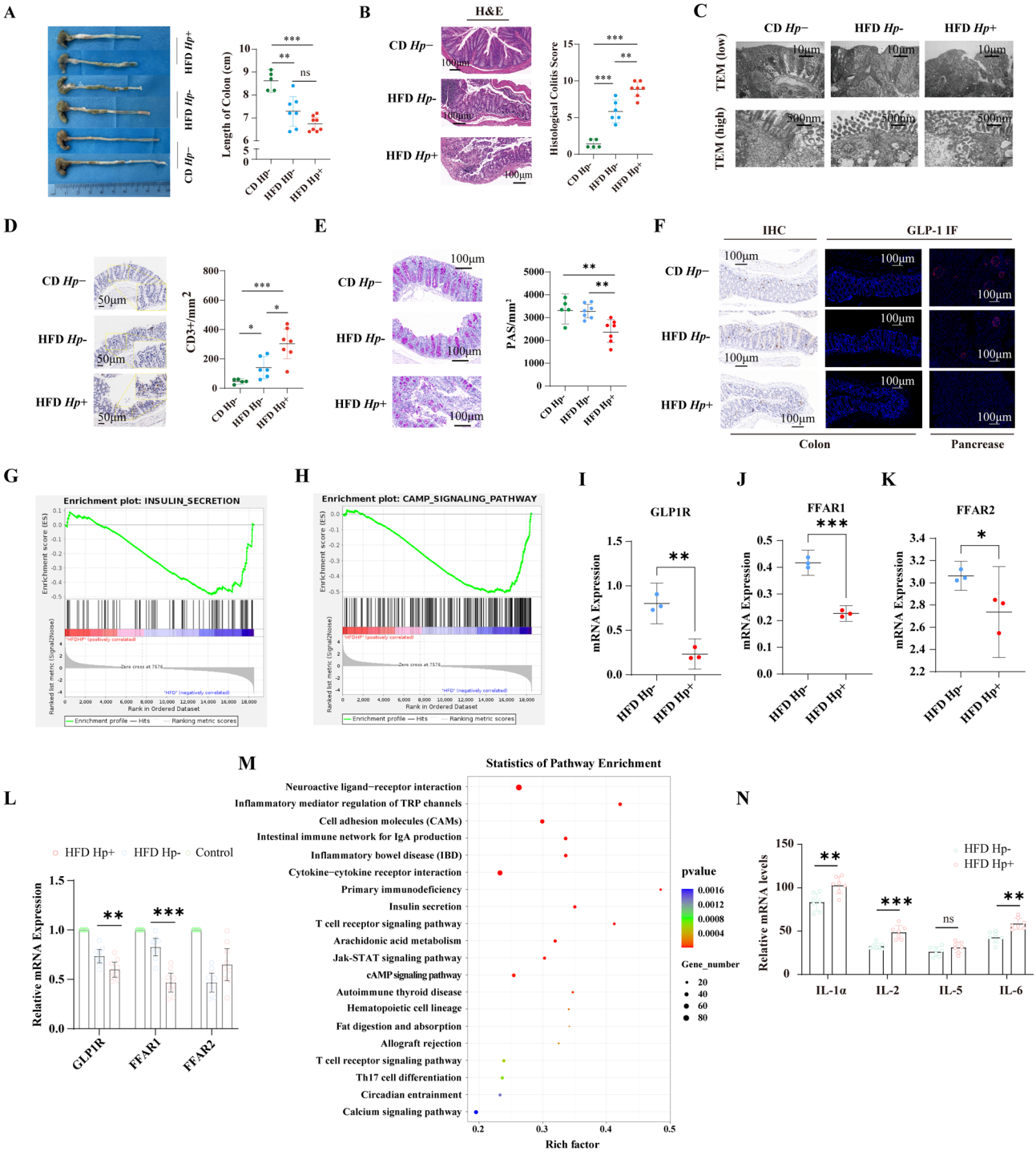

Fig. 2 *Helicobacter* pylori induces inflammatory response and attenuates GLP-1 secretions pathway in the intestine. **A** The colon length; **B** Representative photomicrographs of fixed colon sections after staining with H&E (100 μm), and histological colitis score; **C** Transmission electron microscope of colon Sects. (10 μm and 500 nm). **D** Representative pictures of colonic CD3 + staining and quantification of the CD3 + -positive cells per mm^2. **E** Representative pictures of colonic PAS staining and quantification of the PAS-positive cells per $mm.^2$. **F** Representative pictures of colonic and pancreatic GLP-1R staining. **G** GSEA plot of insulin secretion pathway (**G**), cAMP signaling pathway (**H**) and heatmap of key gene expression in cAMP signaling pathway. **J** relative expression of mRNA in GLP-1R (**J**), FFAR1 (**K**), and FFAR2; **L** Relative mRNA expression of GLP-1R, FFAR1, and FFAR2 in the colon tissue. **M** Bubble chart of KEGG analysis. The Y-axis denotes the pathway names, while the X-axis indicates the enrichment factor, defined as the ratio of the number of differentially expressed genes (DEGs) enriched in a specific KEGG term to the total number of differential genes. A higher ratio signifies a greater degree of enrichment. The size of each bubble corresponds to the number of genes associated with a given pathway, and the color gradient from red to purple reflects the significance level of the enrichment. **N** Relative mRNA expression of IL-1α, IL-2, IL-5 and IL-6 in the colon tissue. *$p < 0.05$, **$p < 0.01$, ***$p < 0.001$

through periodic acid-Schiff (PAS) staining demonstrated a decreased number of goblet cells in the colonic tissue of *H. pylori*-infected diabetic mice compared to uninfected controls (Fig. 2E). Overall, these results indicate that *H. pylori* infection exacerbates colonic inflammation in diabetic mice.

Given the notable reduction in plasma GLP1 levels observed in *H. pylori*-infected diabetic mice, we examined the expression of GLP1-positive epithelial cells in the colon. The number of GLP1-positive cells was significantly lower in *H. pylori*-infected mice compared to uninfected mice (Fig. 2F), consistent with the changes in plasma GLP1 levels. To identify differentially expressed genes (DEGs) following *H. pylori* infection, we conducted RNA sequencing (RNA-seq) analysis on colonic tissue. Subsequent gene set enrichment analysis (GSEA) revealed that the DEGs were significantly enriched in 30 KEGG biological pathways with $|NES| > 1$ and $FDR < 0.05$. Interestingly, the GLP1-dependent intracellular cyclic adenosine monophosphate (cAMP) signal pathway ($NES = -1.77$, $FDR = 0.003$) and insulin secretion pathway ($NES = -1.56$, $FDR = 0.042$) were notably downregulated in *H. pylori*-infected mice compared to uninfected controls (Fig. 2G, H, Table S2). Furthermore, the expression levels of *GLP1R, FFAR1*, and *FFAR2* were significantly reduced in *H. pylori*-infected diabetic mice as identified through RNA-seq (Fig. 2J, K) and were subsequently validated using real-time PCR (Fig. 2). Given the fundamental involvement of inflammatory pathways in the pathophysiology of diabetes, we also examined whether markers related to inflammation of intestinal tissues were altered following *H. pylori* infection. The KEGG analysis revealed significant alterations in the pathways related to the regulation of TRP channels by inflammatory mediators, inflammatory bowel disease (IBD), and the Jak-STAT signaling pathway, with all p-values being less than 0.01. In contrast, the NF-kappa B signaling pathway did not exhibit a significant change ($p = 0.82$) (Fig. 2). Additionally, real-time PCR analysis demonstrated that the expression levels of inflammatory markers *IL-1α, IL-2,* and *IL-6* were significantly elevated in H. pylori-infected diabetic mice (Fig. 2). These results indicates that *H. pylori* exacerbates the intestinal epithelial inflammatory response and attenuates enterogenous GLP-1 secretion-related signals.

H. pylori alters colonic microbial composition and induces microbiota-dependent SFCA transformation, which correlated to disruption of blood glucose homeostasis

Changes in the gastrointestinal microbiome and the abnormal presence of certain types of bacteria have been linked to insulin resistance [27, 28]. Since *H. pylori* infection has been shown to alter the properties of the microbiota, this may be another mechanism by which *H. pylori* aggravates glucose intolerance. Thus, we evaluated the impact of *H. pylori* infection on gastric tissue and colonic microbial composition through 16 s rRNA and shotgun metagenomics sequencing. Our results showed a notable increase in the abundance of *Helicobacter spp.* in both gastric tissue (Figure S2I) and ileocecal contents of mice infected for 10 weeks (Figure S3A-I). To further investigate the nature of *H. pylori* as a transient passer or colonized bacterial in the colon, we cultured the gastric and colonic tissues of *H. pylori* infected mice on separate coated plates. Results showed growth of *H. pylori* in the gastric tissue but not in the colonic tissue (Figure S3G), indicating that *H. pylori* may be a transient flora in the colon rather than a resident bacteria. Interestingly, we observed that the abundance of *Helicobacter* in murine gastric tissue was significantly positively correlated with the presence of the genera *Helicobacter* and various *Helicobacter* species, including *H. pylori*, in intestinal contents (Table S3, Figure S3G). Therefore, *H. pylori* infection in the stomach may directly traverse the gastrointestinal tract, resulting in a notable increase in the abundance of the *Helicobacter* genus within the intestinal contents. Furthermore, results of shotgun metagenomics sequencing showed apparent changes in microbial composition in the colonic environment upon *H. pylori* infection. The refraction curves of the observed species tend to flatten, suggesting that the depth of the sequence has reached saturation (Fig. 3A). While no signs of alpha diversity were observed in terms of species richness, Chao1, and Simpson index after *H. pylori* infection (Fig. 3B), a significant difference in beta diversity (Bray–Curtis distances) was observed in Axis1 of PCoA and Axis2 (Fig. 3C), indicating heterogeneous microbiota distributions between *H. pylori*-infected diabetic mice and uninfected controls. The three groups also showed remarkable differences in the composition of the microflora (Fig. 3D, E). At the phylum level, *Firmicutes* and *Proteobacteria* showed a significant increase, while *Actinobacteria* and *Verrucomicrobia* exhibited a significant decrease in the ileocecal contents of the *H. pylori*-infected diabetic group compared to uninfected controls (Figure S4A). Furthermore, at the genus level, various species of *Helicobacter* showed a significant increase, whereas the presence of SCFA-producing bacterial genera like *Bifidobacterium, Lactobacillus,* and *Akkermansia* decreased significantly (Figure S4B). At the species level, we identified 150 bacterial species, all of which showed a significant increase in *H. pylori*-positive diabetic mice compared to uninfected diabetic or nondiabetic controls (Table S4). The genus *Helicobacter* was the most prevalent among these differential species, with 34 *Helicobacter* strains identified (Fig. 3F). This indicates an increase not only in *H. pylori* but also in *non-H. pylori Helicobacter species* in colon contents following *H. pylori*

infection. Additionally, the microbial co-occurrence network correlation analysis showed a significant negative relationship between the abundance of *Helicobacter* species and SCFA-producing bacteria like *Bifidobacterium* and *Lactobacillus* (Fig. 3G). This suggests that the enrichment of *Helicobacter spp.* in the colon may hinder the growth of beneficial colonic bacteria. RDA redundancy analysis indicated a notable positive correlation between the bacterial flora of *H. pylori*-infected diabetic mice and blood glucose disturbances (Fig. 3H, Table S5). Further Spearman analysis highlighted that the top 50 most significantly different bacterial species following *H. pylori* infection were correlated with glucose homeostasis (Fig. 3I). Specifically, SCFA-producing bacteria like *Bifidobacterium* and *Lactobacillus* exhibited a significant negative correlation with blood glucose disturbances and decreased serum GLP-1 secretion, while *Helicobacter spp.* showed a significant positive correlation (Table S6).

We then conducted a gene-centric analysis of the metagenomic data sets to explore the functional changes in the gut microbiota that might contribute to impaired glucose homoeostasis. Significant functional changes in the gut microbiota were observed in the all three groups (Fig. 4A). Considering the decreased enrichement of SCFA-producing bacteria in *H. pylori*-infected diabetic mice, we specially examined the genes involved in the production of SCFA metabolites. Interestingly, we found that several genes that encode key enzymes to SCFAs production pathways were significantly changed in *H. pylori*-infected diabetic group compared to uninfected controls (Fig. 4B). Thus, we performed SCFA quantitative analysis of colonic contents. The shifts in the abundance of genes encoding the SCFA production pathways were largely consistent with the measured SCFA content. Acetic acid and propionate acid concentrations were remarkably decreased in *H. pylori*-infected diabetic group compared to uninfected controls (Fig. 4C). The RDA redundancy analysis indicated a notable positive correlation between SCFA distrubution of *H. pylori*-infected diabetic mice and blood glucose disturbances (Fig. 4D). Several SCFA-producing bacteria which were significantly decreased in *H. pylori*-infected diabetic group showed a notable positive correlation between SCFA concentrations (Fig. 4E).

The transplanted flora from H. pylori-infected diabetic mice shapes a pro-inflammation and inhibits intestinal GLP-1 secretion

To investigate the impact of *H. pylori*-induced microbiota signatures on insulin resistance, a stool transfer experiment was conducted (Fig. 5A). Stool samples from infected and non-infected specific pathogen-free (SPF) mice were transferred into recipient mice that had been pretreated with broad-spectrum antibiotics (intragastric administration of a quadruple broad-spectrum antibiotic combination including vancomycin 1 g/L, ampicillin 1 g/L, neomycin 1 g/L, and metronidazole 1 g/L) to mimic germ-free conditions (Fig. 5B). After a two-month fecal transplantation period, shotgun metagenomics sequencing revealed similar stool compositions in both donor and recipient mice across the three groups (Fig. 5C, D). The SCFA compositions were also comparable in recipient mice transplanted with fecal supernatant from *H. pylori*-infected mice, showing a notable decrease in total SCFAs, acetic acid, and propionate acid concentrations (Fig. 5E). Although there was no significant weight change (Fig. 5F), mice transplanted with fecal supernatant from *H. pylori*-infected mice exhibited elevated fasting blood glucose levels (Fig. 5G), reduced serum GLP-1 levels (Fig. 5H), and impaired glucose intolerance (Fig. 5I). Furthermore, these mice displayed more severe colonic inflammation, a decrease in PAS-positive cells, disruption of the intestinal mucosal barrier, and a lower number of GLP-1-positive cells (Fig. 5J). Liver tissues of recipients transplanted with fecal supernatant from *H. pylori*-infected mice exhibited lower expression of p-IRS1 (Fig. 5K), suggesting more pronounced hepatic insulin resistance.

To further explore the impact of gut microbiota and microbiota-dependent SCFA generation on intestinal GLP-1 secretion, we conducted experiments on the proglucagon transcription, intracellular cAMP levels, and GLP-1 secretion in STC-1 and NCI-H716 cells. The cells were exposed to four different co-culture conditions for 1 and 24 h, which included fecal supernatant from *H. pylori*-infected diabetic mice, non-*H. pylori*-infected diabetic mice, non-diabetic controls, and *H. pylori*-infected diabetic mice supplemented with SCFAs (acetic acid: propionic acid: butyric acid = 1:1:1). The results revealed no significant difference in GLP-1 production among the groups after 1 h of incubation (Figure S5A, S5B). However, after 24 h, co-culturing with fecal supernatant from *H. pylori*-infected diabetic mice led to a notable decrease in proglucagon transcription, cAMP levels, and GLP-1 secretion in both cell lines (Figure S5C-H). Conversely, the addition of exogenous SCFAs to the fecal supernatant from *H. pylori*-infected diabetic mice resulted in increased proglucagon transcription, cAMP levels, and GLP-1 secretion in both cell lines. These findings suggest that H. pylori infection modifies the composition of the colonic microbiota and stimulates microbiota-dependent SCFA production, which may subsequently suppress intestinal GLP-1 secretion and synthesis by enhancing proglucagon transcription.

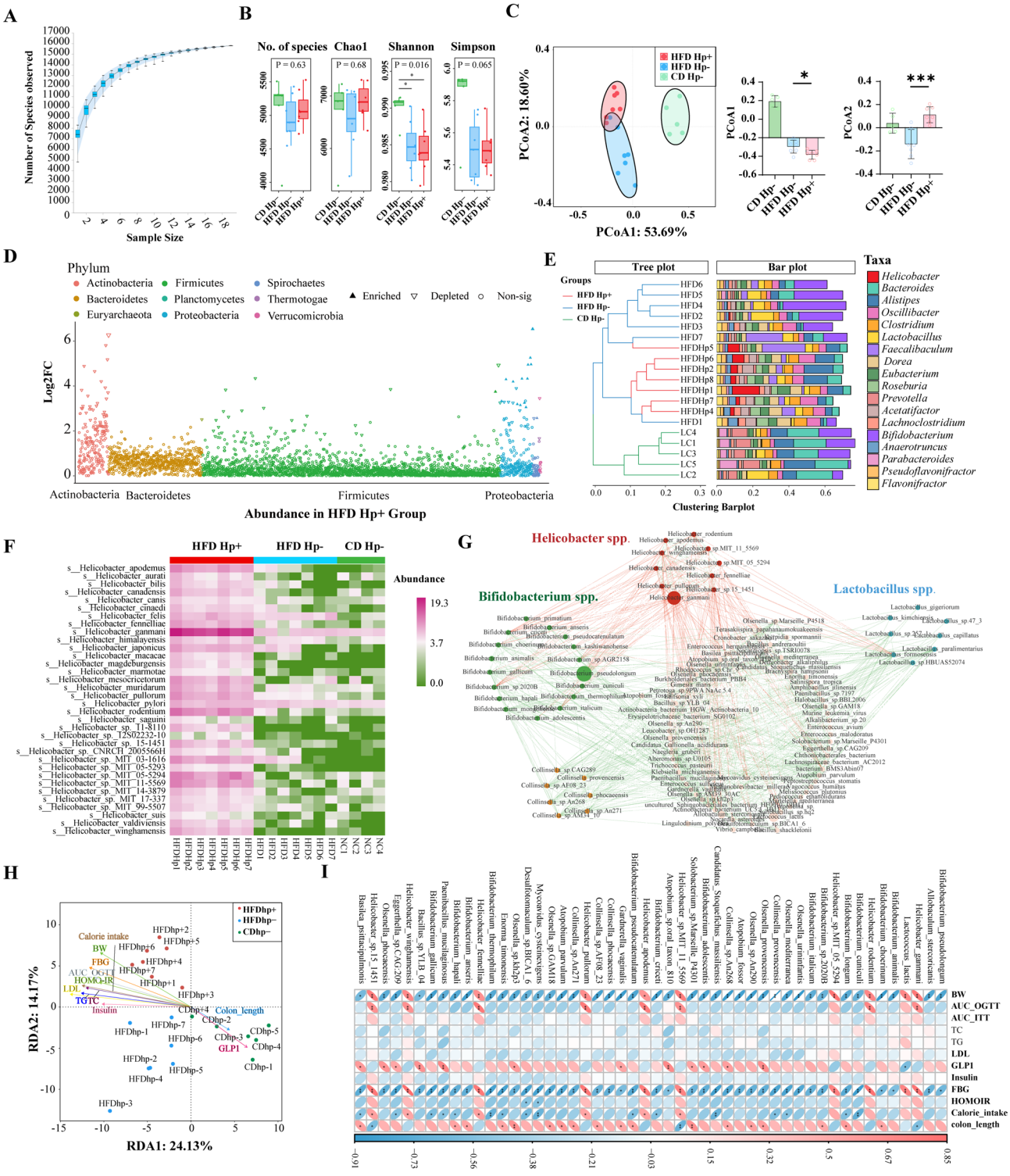

Fig. 3 (See legend on next page.)

H. pylori-induced glucose homeostasis imbalance is alleviated after H. pylori eradication

To investigate the potential impact of eradicating *H. pylori* infection on the pro-diabetic profile, mice were subjected to a triple therapy regimen comprising clarithromycin, rabeprazole, and amoxicillin (Fig. 6A, B). The results showed a significant decrease in body weight and fasting glucose levels in *H. pylori*-infected diabetic mice following antibiotic treatment (Fig. 6C, D), with no notable changes observed in the control groups receiving

(See figure on previous page.)

Fig. 3 *Helicobacter* pylori alters intestinal microbial composition, which is associated with disruption of blood glucose homeostasis. **A** Species accumulation curve. X-axis represents the sample size, Y-axis represents the number of species examined, and blue shading reflects the confidence intervals of the curve; **B** Microbialadiversity index, including the total number of species, Chao1, Shannon and Simpson index; **C** PCoA plot based on Bray–Curtis distances: each point represents one sample, different colored points indicate different groups, the percentage in the Y axis brackets represents the proportion of the sample difference data (distance matrix) that can be explained by the corresponding Y axis; and Distance of each group sample in the X1 axis and the X2 axis of PCoA analysis; **D** Manhattan plot of Microbial distribution: each point represents one strain, and the color represents the different phylum levels. The positive triangle represents the increase of the species abundance in the HFD Hp + group, and the inverse triangle represents the decrease of the species abundance in the HFD Hp + group. **E** Hierarchical cluster plot: the panel on the left is the hierarchical cluster tree graph, where samples cluster according to the similarity between each other, the shorter the branch length, the more similar the two samples; the panel on the right is the stacked bar of the top 18 enrichment species. **F** Heatmap of relative abundance of each fecal *Helicobacter* species significantly enriched in HFD Hp + group. Red represents increased, green represents decreased, the darker the difference in relative abundance; **G** Network diagram of microflora interactions. HFD Hp (+) group of mice in the flora species (species) flora network interaction, red line between the two species is a negative correlation (rho > 0.7), green line indicates positive correlation (rho > 0.7), circle represent each species: the red represent s *Helicobacter* species, the green represents *Bifidobacterium* species, blue represents *Lactobacillus* species. The larger the circle area, the higher the abundance. **G** plot of RDA redundancy analysis: each point represents one sample. Different color points represents different groups. The closer the distance between two points, the higher the flora composition/functional similarity of the two samples. Blue arrows represent different influencing factors, the Angle between the influencing factors represents their positive correlation, the right Angle is unrelated, the blunt angle is negative correlation, the longer the radiation, the greater the influence on the flora composition/function; the blue arrow ray and the coordinate axis represents the correlation of a certain environmental factor and the coordinate axis, the smaller the Angle, the higher the correlation. The position of the projected point of the sample on the blue arrow that approximately represents the numerical size of that factor in the corresponding sample. The percentages in the axis brackets represent the proportion of differences in the original data that can be explained by the corresponding axes. **I** Visualization of Spearman association analysis of significantly changed species in *H. pylori*-infected diabetic mice and the glycemic parameters: blue indicates negative correlation, red indicates positive correlation, and the color depth indicates the strength of correlation; $^{*}p < 0.05$, $^{**}p < 0.01$, $^{***}p < 0.001$

a placebo. Moreover, mice that underwent eradication exhibited longer total colon length, reduced histological colitis scores, and higher numbers of goblet cells and GLP-1 positive cells in colonic tissue compared to those in the non-eradication groups (Fig. 6E-I). The glucose intolerance and insulin resistance were notably improved in diabetic mice after *H. pylori* eradication (Fig. 6J-K). Furthermore, liver microvesicular steatosis and infiltrating macrophages (F4/80-positive cells) were alleviated in diabetic mice following *H. pylori* eradication (Fig. 6L). The ratio of IRS1/p-IRS1 was significantly lower in *H. pylori*-eradicated diabetic mice (Fig. 6M), indicating an enhancement in hepatic insulin signaling and a reduction in hepatic insulin resistance.

Discussion

This study presents a novel gut microbiota-mediated mechanism of how *H. pylori* infection can lead to an imbalance in glucose homeostasis. We initially established a retrospective cohort study that confirmed previous findings linking *H. pylori* infection to worsened blood sugar control in patients with T2D. Using mouse models induced with a high-fat diet and low-dose streptozotocin (HFD + STZ) to mimic T2D, we found increased insulin resistance in *H. pylori*-infected mice, consistent with epidemiological data. This prompted further investigation into the potential mechanisms responsible for the glucose dysregulation caused by *H. pylori*. Our research revealed that *H. pylori* infection resulted in shifts in the intestinal microbial community, marked by an increase in LPS-producing bacteria and a decrease in SCFA-producing bacteria. Specifically, after administering *H. pylori* orally to diabetic mice, a notable increase in *Helicobacter* abundance was observed in colonic contents, including *H. hepaticus*, *H. bilis*, and *H. helimannii*, known for their pathogenic potential. These species were reported to be linked to a higher risk of MALT lymphoma compared to *H. pylori* [29]. Additionally, *H. hepaticus, H. muerneri, and H. bilis* were found to harbor multiple virulence genes that not only trigger animal diseases but also heighten susceptibility to Crohn's disease and ulcerative colitis [30]. Therefore, the increased abundance of colonic *Helicobacter* species post *H. pylori* infection could lead to a rise in harmful intestinal bacteria, ultimately impacting the intestinal microenvironment. Furthermore, we observed a positive correlation between the increased abundance of colonic *Helicobacter* species and higher blood glucose levels, suggesting a potential connection between colonic *Helicobacter* species and metabolic disorders. Previous studies have indicated that colonic *Helicobacter* species could serve as a potential biomarker of obesity in mouse models [30]. Another study also demonstrated that mice lacking fat mass and obesity-related genes (Fto) exhibited specific bacterial profiles that suppress inflammation, characterized by reduced abundance of the *Porphyromonas* family and *Helicobacter* genus, and increased levels of lactobacillus [31]. This aligns with the microbiota changes observed in our study that decreased abundance of beneficial bacteria such as bifidobacterium and Lactobacillus were presented after *H. pylori* infection. Thus, it is possible that the increase in colonic *Helicobacter* abundance due to *H. pylori* infection may inhibits the growth of SCFA-producing bacteria and ultimately causing disruptions in intestinal flora.

We also found that the production of intestinal SCFA metabolites decreased after *H. pylori* infection, leading to

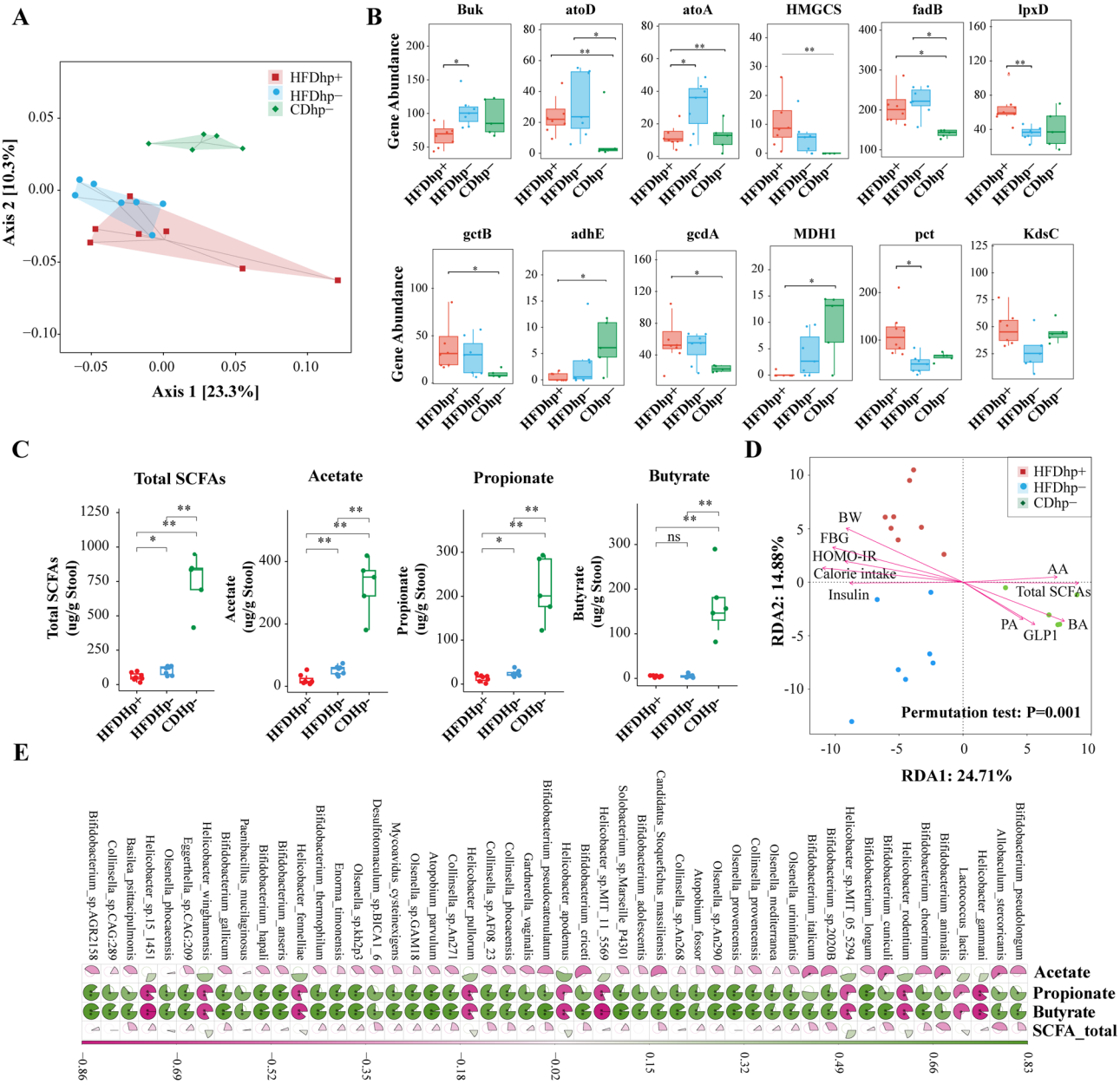

Fig. 4 *Helicobacter* pylori induces decreased the generation of cecal SCFAs, which further disrupts the GLP-1 secretion. **A** PCoA plot based on Bray–Curtis distances of metagenomic functional annotation. Each point represents a cecal content sample, each color represents different groups; **B** Microbial gene expression: the X axis represents different groups of mice, the Y axis represents the expression of annotated microbial genes. **C** Box plot of cecal targeted SCFA concentration, including total SCFAs, acetate, propionate and butyrate; **D** plot of RDA Redundancy analysis: Each point represents one sample, and points of different colors belong to different groups. The closer the distance between two points is, the higher the similarity of the SCFA composition characteristics of the two samples. Blue arrows represent different influencing factors, the Angle between the influencing factors represents the positive correlation between the two factors, the right Angle is unrelated, the obtuse angle is negative correlation, the longer the radiation, indicates that the factor affects the SCFA; the blue arrow ray and the coordinate axis represents the correlation of a certain environmental factor and the coordinate axis, the smaller the Angle, the higher the correlation. The position of the projected point of the sample on the blue arrow that approximately represents the numerical size of that factor in the corresponding sample. The percentages in the axis brackets represent the proportion of differences in the original data that can be explained by the corresponding axes. **E** Visualization of Spearman association analysis of SCFA and blood glucose indicators: green indicates negative correlation, red indicates positive correlation, $*p < 0.05$, $**p < 0.01$, $***p < 0.001$

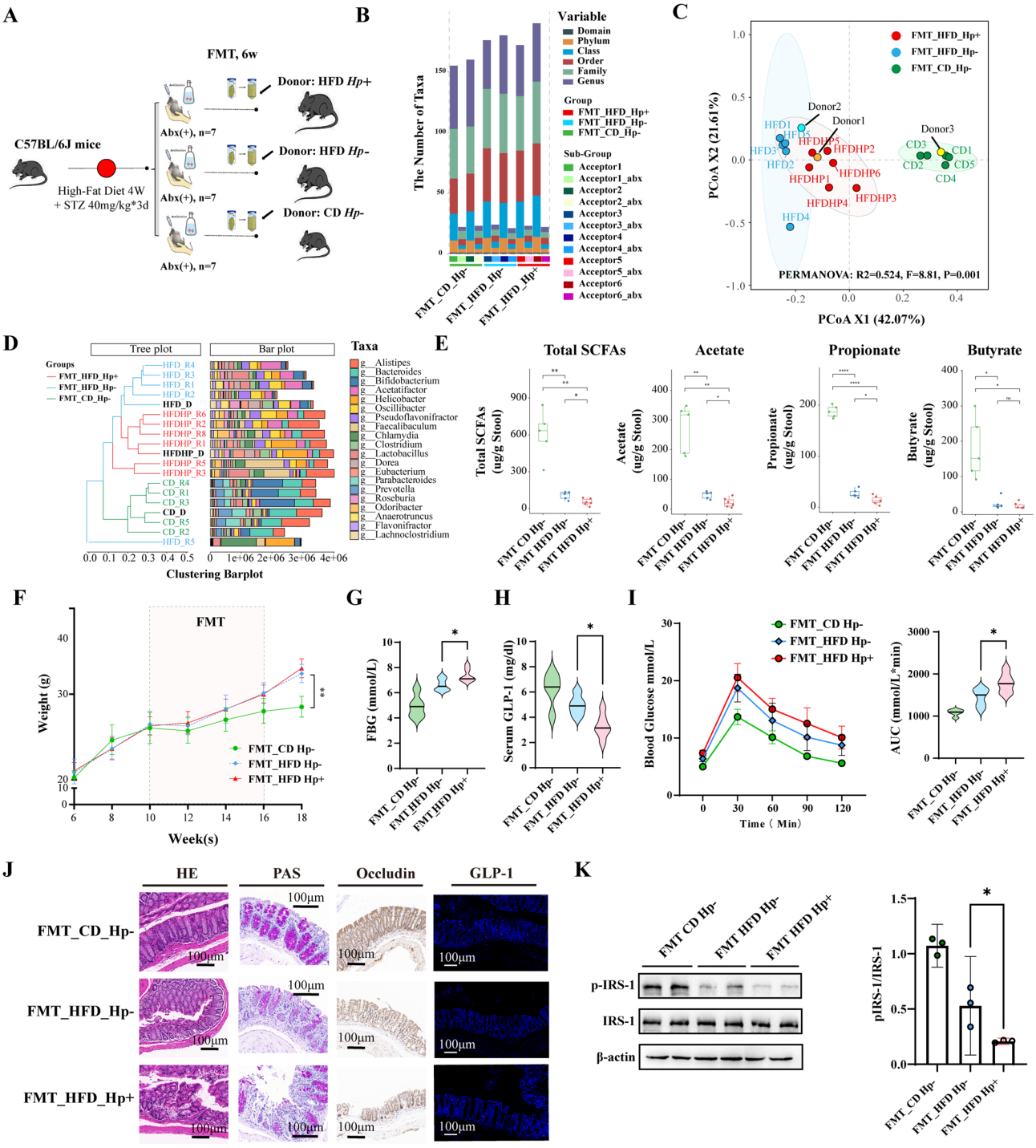

Fig. 5 The altered gut mocrobiome after *Helicobacter pylori* infection aggregates insulin resistance and decreases GLP-1 secretion in antibiotic-treated mouse model. **A** Schematic diagram of FMT experiment design; **B**. Bar chart of fecal microbial count of antibiotic-treated mice before and after FMT; **C** PCoA plot based on Bray–Curtis distances of cecal microbial composition of representative donor and recipient mice. **D** Hierarchical cluster plot of cecal microbial composition of the donor (D) and recipient (R) mice in each group after FMT; **E** Box plot of cecal targeted SCFA concentration, including total SCFAs, acetate, propionate and butyrate, in FMT recipient mice; **F** Body weight change; **G** fasting blood glucose; **H** Serum GLP-1 levels; **I** Blood glucose levels and AUC of OGTT; **J** Representative photomicrographs of fixed colon sections after staining with H&E (100 μm), PAS staining, Occludin staining, and GLP-1R immunofluorescence; **K** IRS-1 and p-IRS-1 protein expression in the liver tissue. *$p < 0.05$, **$p < 0.01$, ***$p < 0.001$

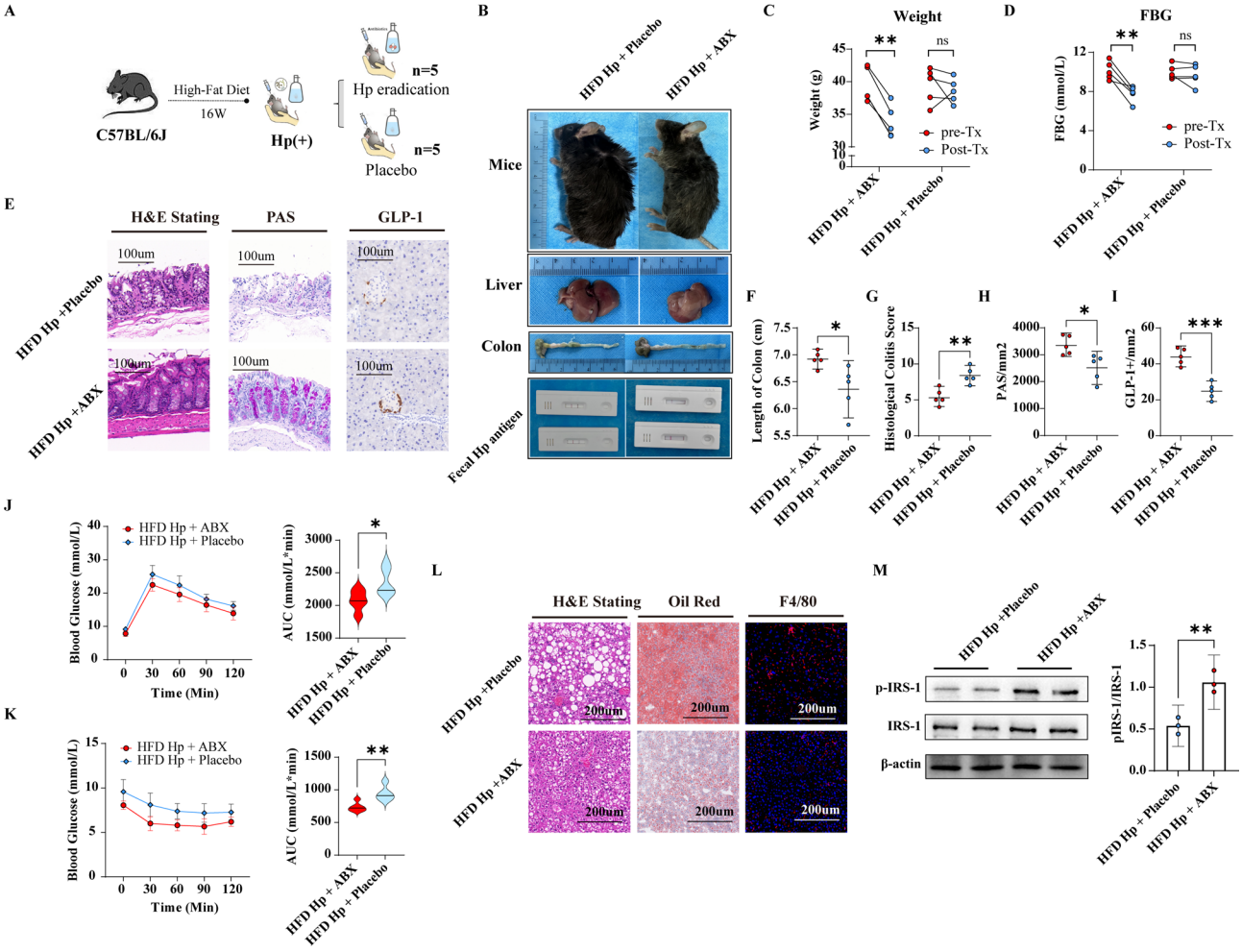

Fig. 6 *Helicobacter pylori*-induced colonic inflammation and insulin resistance are attenuated by eradication. **A** Schematic diagram of experiment design; **B** Comparison of gross and visceral morphology between the two groups after eradication of 8W; **C** Paired scatter plot of body weight changes before and after eradication; **D** Paired scatter plot of fasting blood glucose changes before and after eradication; **E** Representative photomicrographs of fixed colon sections and pancreas after staining with H&E (100 μm), PAS staining (100 μm), and GLP-1R immunofluorescence (100 μm); **F**-**I** Scatter plot of colon length (**F**), pathological colitis score (**G**), PAS positive cells per mm^2 (**H**), and GLP-1 positive cells per $mm.^2$ (**I**); **J** Blood glucose levels and AUC of OGTT; **K** blood glucose levels of ITT; **L** Representative photomicrographs of fixed liver sections after staining with H&E (200 μm), ORO (200 μm), F4/80 antibody (200 μm). M. IRS-1 and p-IRS-1 protein expression in the liver tissue. *$p < 0.05$, **$p < 0.01$, ***$p < 0.001$

a significant reduction in propionic acid and acetic acid levels. Normally, propionate and acetate are absorbed into the portal venous circulation and utilized by various tissues, particularly the liver, for energy metabolism. Additionally, SCFA can interact with G protein-coupled receptors on intestinal epithelial cells, impacting metabolism and GLP-1 production. Immunohistochemistry and immunofluorescence analyses revealed a decrease in GLP-1-positive cells in colon tissue and pancreas post *H. pylori* infection, accompanied by a significant drop in serum GLP-1 levels. Notably, GLP-1 levels increased significantly following *H. pylori* eradication compared to non-eradicated individuals, suggesting improvements in carbohydrate metabolism [32]. Changes in intestinal microecology pre and post eradication may play a crucial role in regulating GLP-1 secretion. A clinical study from Malaysia demonstrated a significant rise in GLP-1 levels at 0, 6, and 12 months post *H. pylori* eradication [17]. These studies are consistent with our findings, indicating that mRNA expression levels of FFAR1 and GLP-1R were down-regulated in the colon tissue of mice following *H. pylori* infection. FFAR1 and GLP-1R are targets of SCFA-activated L cells for GLP-1 secretion. The decreased expression of these genes post-infection may contribute to the reduction in GLP-1 secretion. However, further research is needed to confirm whether GLP-1 levels fluctuate after *H. pylori* infection or eradication, and their role in regulating insulin resistance in T2D.

Furthermore, we utilized Fecal Microbiota Transplantation (FMT) to investigate the potential link between *H. pylori* infection and the onset of metabolic diseases. FMT serves as a valuable tool for examining the

cause-and-effect relationship between gut flora and specific traits, offering a robust means to validate the causal involvement of particular bacteria or microbial communities in disease pathogenesis [22, 33]. Our research demonstrated that mice receiving fecal transplants from *H. pylori*-infected mice exhibited similar characteristics of blood sugar dysregulation to the original donors, confirming that alterations in gut flora induced by *H. pylori* play a significant role in impacting blood glucose levels and insulin sensitivity. Notably, this approach represents a novel contribution to the existing literature on *H. pylori* infection and gut microbiota, shedding light on the crucial intermediary role of gut flora in exacerbating insulin resistance associated with *H. pylori* infection. Interestingly, we observed that both direct administration of *H. pylori* and transplantation of the intestinal microbiota from *H. pylori*-infected mice into antibiotic-treated, sterilized mice resulted in a reduction of certain SCFA-producing bacteria, including *Bifidobacterium* and *Lactobacillus*, and an increase in LPS-producing bacteria, particularly *Helicobacter spp*. We hypothesize that these microbial shifts may serve as potential modulators connecting *H. pylori* infection to insulin resistance.

This study does have some limitations. Firstly, the retrospective cohort study utilized a single-center cohort with a relatively small sample size, potentially impacting statistical power. Based on this retrospective study, we are presently unable to ascertain whether there exist potential intestinal pathogenic bacterial populations that may interact with *H. pylori* to exacerbate glucose metabolism disorders in diabetic patients. Consequently, our clinical research is limited to confirming an association between *H. pylori* and suboptimal glycemic control in diabetic individuals. To elucidate the causal relationship and assess the impact of other pathogens on diabetes, further investigation is warranted. Additionally, the mouse experiment involved antibiotic-sterilized mice instead of germ-free mice, which could have influenced the experimental outcomes. Furthermore, the FMT was not conducted in an anaerobic workstation. Although efforts were made to create an anaerobic environment during the transplantation process by using daily transplantation of fresh feces and anaerobic bags, there may still be some impact on the transplantation results. Furthermore, the *H. pylori SS1* strain utilized in this study is deficient in the cag pathogenicity island (cagPAI). Given that Type-I cagPAI-positive *H. pylori* strains are the most virulent in human infections, this study did not specifically investigate the effects of infection with cagA-positive *H. pylori* strains on blood glucose metabolism. This aspect warrants further investigation in future experimental designs.

In conclusion, our study revealed that *H. pylori* infection can impact the abundance of SCFA-producing bacteria and decrease the levels of SCFAs within the intestines. Furthermore, *H. pylori* is observed to exacerbate the intestinal epithelial inflammation and attenuates enterogenous GLP-1 secretions. The eradication of *H. pylori* significantly alleviated intestinal inflammation and improved the imbalance in glucose homeostasis. This research offers a fresh perspective on investigating the link between *H. pylori* infection and metabolic disorders. Therefore, incorporating *H. pylori* status into preventive strategies for diabetes should be taken into account.

Abbreviations

H. pylori	Helicobacter pylori
T2D	Type 2 Diabetes
HbA1c	Fasting blood glucose and glycated hemoglobin
SCFAs	Short chain fatty acids
GLP-1	Glucagon-like peptide-1
13C-UBT	13C urease breath test
OGTT	Oral Glucose Tolerance Test
BMI	Body Mass Index
FBG	Fasting Blood Glucose
TC	Total cholesterol
TG	Total triglycerides
Hp-SS1	*H. pylori* Sydney strain
HFD	High-fat diet
ASVs	Amplicon sequence variants
LEfSe	Linear discriminant analysis effect size
SRA	Sequence Read Archive
MENAs	Molecular ecological network analyses
RMT	Random matrix theory
IRS	Insulin receptor substrate
cAMP	Cyclic adenosine monophosphate
IBD	Inflammatory bowel disease
SPF	Specific pathogen-free
FMT	Fecal Microbiota Transplantation
cagPAI	Cag pathogenicity island

Supplementary Information

The online version contains supplementary material available at https://doi.org/10.1186/s12866-025-04402-9.

Supplementary Material 1.

Supplementary Material 2.

Supplementary Material 3.

Supplementary Material 4.

Authors' contributions

Han Chen: study concept and design, analysis and interpretation of data; drafting of the manuscript, authorship; Xiaoying Zhou and Wei Su: study concept and design, analysis and interpretation of data, authorship. Zi Wang, Qiang Ye, Shuo Li: anmial study, data extraction, design and order the figures and tables, assessment of study quality, authorship. Guoxin Zhang: design and order the figures and tables, assessment of study quality, authorship. Xiaoying Zhou: critical revision of the manuscript for important intellectual content; obtain funding; study supervision, authorship.

Funding

This study was granted by the National Natural Science Foundation of China (No. 82100594).

Data availability

All the metagenomic raw data have been submitted to the Sequence Read Archive (SRA) in NCBI (Archive number: PRJNA1139859). In addition, all

data from this study can be obtained from the corresponding author upon reasonable request.

Declarations

Ethics approval and consent to participate

The study was approved by the Institutional Ethics Committee of the First Affiliated Hospital of Nanjing Medical University and was then registered in the Chinese Clinical Trial Registry center (www.chictr.org.cn; registration No. ChiCTR2200063489). Informed consent was obtained from each subject enrolled. All experiments were performed in accordance with relevant guidelines and regulation.

Competing interest

The authors declare no competing interests.

Received: 7 April 2025 / Accepted: 15 September 2025
Published online: 14 October 2025

References

1. Hooi JKY, Lai WY, Ng WK, et al. Global prevalence of *Helicobacter pylori* infection: systematic review and meta-analysis. Gastroenterology. 2017;153:420–9.
2. Tsay FW, Hsu PI. H. pylori infection and extra-gastroduodenal diseases. J Biomed Sci. 2018;25(1):65.
3. Gloyn AL, Drucker DJ. Precision medicine in the management of type 2 diabetes. Lancet Diabetes Endocrinol. 2018;6(11):891–900.
4. Yao CC, Kuo CM, Hsu CN, et al. First-line Helicobacter pylori eradication rates are significantly lower in patients with than those without type 2 diabetes mellitus. Infect Drug Resist. 2019;12:1425–31.
5. Li J-Z, Li J-Y, Wu T-F, et al. *Helicobacter pylori* infection is associated with type 2 diabetes, not type 1 diabetes: an updated meta-analysis. Gastroenterol Res Pract. 2017;2017:5715403.
6. Gunji T, Matsuhashi N, Sato H, Fujibayashi K, Okumura M, Sasabe N, et al. *Helicobacter pylori* infection significantly increases insulin resistance in the asymptomatic Japanese population. Helicobacter. 2009;14(5):144–50.
7. Wan Z, Song L, Hu L, Hu M, Lei X, Huang Y, et al. *Helicobacter pylori* infection is associated with diabetes among Chinese adults. J Diabetes Investig. 2020;11(1):199–205.
8. Kato M, Toda A, Yamamoto-Honda R, et al. Association between *Helicobacter pylori* infection, eradication and diabetes mellitus. J Diabetes Investig. 2019;10(5):1341–6.
9. Song X, Cai C, Jin Q, et al. The efficacy of *Helicobacter pylori* eradication in diabetics and its effect on glycemic control: a systematic review and meta-analysis. Helicobacter. 2021;26(2):e12781.
10. Roca-Rodríguez MM, Coín-Aragüez L, Cornejo-Pareja I, et al. Carbohydrate metabolism improvement after *Helicobacter pylori* eradication. Diabetes Metab. 2016;42(2):130–4.
11. Schulz C, Schütte K, Koch N, et al. The active bacterial assemblages of the upper GI tract in individuals with and without Helicobacter infection. Gut. 2018;67(2):216–25.
12. The human gastric microbiome is predicated upon infection with Helicobacter pylori. Front Microbiol. 2017;8:2508.
13. Chen CC, Liou JM, Lee YC, et al. The interplay between Helicobacter pylori and gastrointestinal microbiota. Gut Microbes. 2021;13(1):1–22.
14. Chen X, Wang N, Wang J, et al. The interactions between oral-gut axis microbiota and Helicobacter pylori. Front Cell Infect Microbiol. 2022;3(12):914418.
15. Martin-Nuñez GM, Cornejo-Pareja I, Clemente-Postigo M, et al. Gut Microbiota: The Missing Link Between Helicobacter pylori Infection and Metabolic Disorders? Front Endocrinol (Lausanne). 2021;17(12):639856.
16. Huang Y, Ding Y, Xu H, Shen C, Chen X, Li C. Effects of sodium butyrate supplementation on inflammation, gut microbiota, and short-chain fatty acids in *Helicobacter pylori*-infected mice. Helicobacter. 2021;26(2):e12785.
17. Yap TW, Leow AH, Azmi AN, et al. Changes in metabolic hormones in Malaysian young adults following Helicobacter pylori eradication. PLoS One. 2015;10(8):e0135771.
18. Drucker DJ. Mechanisms of action and therapeutic application of glucagon-like peptide-1. Cell Metab. 2018;27(4):740–56.
19. Chen XY, Chen L, Yang W, et al. GLP-1 Suppresses Feeding Behaviors and Modulates Neuronal Electrophysiological Properties in Multiple Brain Regions. Front Mol Neurosci. 2021;17(14):793004.
20. Aroda VR. A review of GLP-1 receptor agonists: evolution and advancement, through the lens of randomised controlled trials. Diabetes Obes Metab. 2018;20(Suppl 1):22–33.
21. Cornejo-Pareja I, Martín-Núñez GM, Roca-Rodríguez MM, et al. H. pylori eradication treatment alters gut microbiota and GLP-1 secretion in humans. J Clin Med. 2019;8(4):451.
22. Thomas JC, Khoury R, Neeley CK, Akroush AM, Davies EC. A fast CTAB method of human DNA isolation for polymerase chain reaction applications. Biochemical Education. 1997;25:233–5.
23. Segata N, Izard J, Waldron L, Gevers D, Miropolsky L, Garrett WS, et al. Metagenomic biomarker discovery and explanation. Genome Biol. 2011;12:R60.
24. Dhariwal A, Chong J, Habib S, King IL, Agellon LB, Xia J. MicrobiomeAnalyst: a web-based tool for comprehensive statistical, visual and meta-analysis of microbiome data. Nucleic Acids Res. 2017;45(W1):W180–8.
25. Ralser A, Dietl A, Jarosch S, Engelsberger V, Wanisch A, Janssen KP, et al. *Helicobacter pylori* promotes colorectal carcinogenesis by deregulating intestinal immunity and inducing a mucus-degrading microbiota signature. Gut. 2023;72(7):1258–70.
26. Engelsberger V, Gerhard M, Mejías-Luque R. Effects of *Helicobacter pylori* infection on intestinal microbiota, immunity and colorectal cancer risk. Front Cell Infect Microbiol. 2024;14:1339750.
27. Soto M, Herzog C, Pacheco JA, Fujisaka S, Bullock K, Clish CB, et al. Gut microbiota modulate neurobehavior through changes in brain insulin sensitivity and metabolism. Mol Psychiatry. 2018. https://doi.org/10.1038/s41380-018-0086-5.
28. Vliex LMM, Penders J, Nauta A, Zoetendal EG, Blaak EE. The individual response to antibiotics and diet - insights into gut microbial resilience and host metabolism. Nat Rev Endocrinol. 2024;20(7):387–98.
29. Ménard A, Smet A. Review: other *Helicobacter* species. Helicobacter. 2019;24(Suppl 1):e12645.
30. Liu D, Wen B, Zhu K, et al. Antibiotics-induced perturbations in gut microbial diversity influence metabolic phenotypes in a murine model of high-fat diet-induced obesity. Appl Microbiol Biotechnol. 2019;103:5269–83.
31. Sun L, Ma L, Zhang H, et al. Fto deficiency reduces anxiety- and depression-like behaviors in mice via alterations in gut microbiota. Theranostics. 2019;9:721–33.
32. Zhao L, Zhang F, Ding X, et al. Gut bacteria selectively promoted by dietary fibers alleviate type 2 diabetes. Science. 2018;359(6380):1151–6.
33. Benech N, Barbut F, Fitzpatrick F, Krutova M, Davies K, Druart C, et al. Update on microbiota-derived therapies for recurrent *Clostridioides difficile* infections. Clin Microbiol Infect. 2024;30(4):462–8.

Publisher's Note